Mon. Not. R. astr. Soc. (1986) **221,** 931–945

Pair-induced spectral changes and variability in compact X-ray sources

A. C. Fabian,[1] R. D. Blandford,[2] P. W. Guilbert,[1] E. S. Phinney[2] and L. Cuellar[3]

[1] *Institute of Astronomy, Madingley Road, Cambridge CB3 0HA*
[2] *Theoretical Astrophysics 130–33, Caltech, Pasadena, CA 91125, USA*
[3] *Department of Astronomy, University of Chicago, Chicago, IL 60637, USA*

Accepted 1986 March 21. Received March 21; in original form 1986 February 26

Summary. Inverse Compton scattering of ultraviolet photons by GeV electrons produces γ-rays which in turn create electron–positron pairs if the source is sufficiently compact. The pairs modify the emergent radiation spectrum through their own inverse Compton scattering and through thermal Comptonization after they have cooled to sub-relativistic temperatures. Recent calculations of spectral reprocessing under these conditions are extended to situations in which the Thomson optical depth of the pair plasma exceeds unity, and to demonstrate time-dependent behaviour explicitly. The relevance of our results to X-ray observations of active galactic nuclei, binary X-ray sources and γ-ray bursters is discussed briefly.

1 Introduction

Observations of active galactic nuclei have shown that X-rays often account for a substantial fraction of their bolometric luminosity. Most Seyfert I galaxies appear to have power-law X-ray spectra which extend from $\lesssim$1 to $\gtrsim$100 keV, with an energy index $\alpha \simeq 0.7 \pm 0.1$ (e.g. Mushotzky 1982; Rothschild *et al.* 1983; Petre *et al.* 1984). The situation with quasars is less clear because most of them are too faint to be detected at high energy, but recent analyses of *Einstein Observatory* IPC data indicate that the X-ray spectra of some radio-loud quasars are similar to those of Seyfert I galaxies (e.g. Elvis & Lawrence 1985). Some galactic X-ray binaries, such as Cygnus X-1, have similar hard spectra (Sunyaev & Trümper 1979; White, Fabian & Mushotzky 1984).

The widespread occurrence of this spectrum suggests that a fairly robust general mechanism is responsible. Inverse Compton scattering of lower energy (generally UV) photons by relativistic electrons has commonly been invoked as the X-ray emission process. This requires that the electrons have a power-law distribution function $N_\gamma \propto \gamma^{-2.4}$, similar to that observed in galactic cosmic rays and inferred in non-thermal radio sources. It is therefore natural to suppose that the same particle acceleration mechanism (e.g. acceleration by shock waves) is responsible.

Unfortunately, there are good reasons for believing that the situation must be more complicated than this. Rapid ($t_{var} \lesssim 1$ hr) variability has been reported in a few Seyfert galaxies (e.g. Tennant *et al.* 1981; Lawrence *et al.* 1985) and moderate ($t_{var} \sim$ few day) variability is apparently present in most cases (Barr & Mushotzky 1986). In these galaxies the X-ray 'compactness parameter' $l_x = F_x \sigma_T R / m_e c^3$, where R is the minimum source dimension and F_x is the X-ray flux leaving the source, exceeds unity. The Compton cooling time for an electron of energy $\gamma m_e c^2$, $t_{ic} \approx R/\gamma c l_x$, is then inevitably much shorter than the light crossing time (R/c) and so the injected electron distribution function within these X-ray sources must be flatter (by one power of γ) than the steady-state distribution function. This contrasts with the radio sources where there is presumed to be no such difference.

If the X-ray spectra extend beyond MeV energies with a spectral index <1 then the γ-ray compactness parameter $l_\gamma \sim l_x > 1$. γ-rays of energy ≥ 0.5 MeV can then create pairs in collisions with other photons (the cross-section $\sim \sigma_T$) and a source with $l_\gamma > 1$ will be optically thick to this process. This can significantly deplete the emergent γ-ray power so that it is much less than the luminosity of γ-rays produced within the source. In other words, pair production may be important within a source even when the value of l_γ inferred from observation is less than unity. Furthermore, as the pair annihilation cross-section is also $\sim \sigma_T$, the steady-state optical depth to Thomson scattering by cooled electrons and positrons within the source must also be of order unity. Thermal Comptonization can then, strongly distort the UV and X-ray spectrum (Guilbert, Fabian & Rees 1983).

The simplest type of source to envisage is a homogeneous region of size, R, irradiated throughout by soft photons, and within which ultrarelativistic electrons are continuously accelerated. The proportion of secondary pairs created (i.e. those due to photon–photon interactions) increases with the γ-ray compactness parameter l_γ. The pairs provide a further source of inverse Compton X-rays which distorts and softens the observed spectrum (Bonometto & Rees 1971). They may also create their own γ-rays which produce further generations of pairs, i.e. a cascade may develop. Almost all of the electrons and positrons that are created cool to sub-relativistic energies before annihilating. They should have time to equilibrate to the Compton temperature defined by the radiation field and, in so doing, modify the UV and X-ray spectrum.

The possibility that photo-production of electron–positron pairs might be occurring in compact X-ray sources has long been recognized (e.g. Jelley 1966; Herterich 1974; Cavallo & Rees 1978; see also the review by Svensson 1986). The first serious discussion of the steady spectrum was by Bonometto & Rees (1971) who argued that if $l_\gamma > 1$ and if there is a pair-production cascade, the steady-state electron distribution at energies where the source is optically thick to pair production must satisfy $N_\gamma \propto \gamma^{-3}$. In this limit, the inverse Compton γ-ray photon-injection spectrum $S_\varepsilon \propto \varepsilon^{-2}$, where ε is the photon energy measured in units of $m_e c^2$. The injected-electron spectrum satisfies $Q_\gamma \propto \gamma^{-2}$ which gives $N_\gamma \propto \gamma^{-3}$ in a steady state (*cf.* also Kazanas 1984).

More recently, Zdziarski & Lightman (1985) have presented calculations of the emergent spectrum where the X-ray and γ-ray compactness parameters are small enough that secondary particle production can be handled as perturbations, and the pair plasma does not become optically thick to Thomson scattering. They verify that, when the primary electrons are injected mono-energetically at high energy, they cool to establish a steady spectrum $N_\gamma \gtrsim \gamma^{-2}$ and the secondary pairs steepen this distribution function to give an emergent X-ray spectrum whose spectral index increases from $\alpha \simeq 0.5$ to the Bonometto & Rees value $\alpha \simeq 1$ as the X-ray compactness parameter l_x is increased from 10^{-3} to ~ 1. They also found that if the primary electrons are injected with a power-law distribution then the distortion by the secondary pairs is less noticeable.

The rapid cooling of relativistic electrons requires that they are accelerated impulsively

throughout the source region. For example, in the case of a Seyfert galaxy with $l_x \simeq 10$, $R/c \simeq 10^4$ s, the cooling time for a ~ 1 GeV electron is $\leqslant 1$ s and the acceleration must occur on a shorter time-scale than this. Electrostatic acceleration is a plausible way of effecting this and an electric field of $\sim 0.1\,\mathrm{V\,cm^{-1}}$ is required. Strong electric fields have been invoked near spinning black holes on quite independent grounds. In a black hole magnetosphere (Blandford & Znajek 1977; Phinney 1983) magnetic fields, $B \sim 10^4$ G, generated by external currents cross the horizon of the hole and electric fields $E \lesssim 3 \times 10^6\,\mathrm{V\,cm^{-1}}$ will be induced in the magnetosphere. A vacuum magnetosphere is unstable to γ-ray induced pair-production discharge and this is likely to occur throughout the magnetosphere at a sufficient rate to short out the accelerating electric fields. This provides an explanation for why the acceleration is just powerful enough for pair production to be important. The power dissipated in this way will be principally derived from the spin of the hole and an inner accretion disc. Alternatively shock wave acceleration or similar Fermi processes may be responsible but it is hard to sustain the necessary fast relative motion in an electron–positron plasma when the radiative drag is so strong, e.g. Blandford & McKee (1977). When the acceleration is powerful enough to double the electron's energy every gyroperiod, radiation reaction losses will limit the Lorentz factor to a value $\sim 10^6 (B/10^4\,\mathrm{G})^{-1/2}$.

In the present paper, we describe calculations which combine the approaches of Guibert *et al.* (1983) and Zdziarski & Lightman (1985) and compute the self-consistent spectrum from a pair plasma of arbitrary (but self-consistently produced) optical depth. Our approach is necessarily numerical. We solve model kinetic equations for the electrons (and henceforth we understand this to mean electrons plus positrons in equal numbers) and photons including injection, escape, pair production and annihilation, inverse Compton scattering and thermal Comptonization. We assume that any electron escape can be ignored and that dynamical effects, in particular adiabatic losses, can be similarly neglected. Radiative transfer is handled in the crudest possible manner via an escape-probability formalism. Any more detailed treatment must depend upon the shape of the source. We believe that our results are most sensitive to our handling of the radiative transfer and this therefore provides a limit to the sophistication with which we need treat the other microphysical processes.

Preliminary discussions of this combined approach to Comptonization by pair plasmas are contained in Fabian (1984, 1985), Blandford (1984) and Cuellar (1984, unpublished report).

2 Physical processes in a relativistic plasma

2.1 KINETIC EQUATIONS

Our method is to write down different kinetic equations for the electrons and photons that explicitly conserve energy. We then estimate the transition probabilities between the different electron and photon energy bins. All of the processes that we discuss are elementary in the sense that their cross-sections are accurately known. Unfortunately they are cumbersome to calculate at mildly relativistic energies. In view of the uncertainty in the radiation transfer, approximate expressions suffice. We verify after the fact that there is little energy transfer where the approximations are known to be poor, and that our results are insensitive to those approximations. The numerical method is sufficiently accurate that these model equations can be used to examine time-dependent behaviour.

It is convenient to choose electron energy γ (in units of $m_e c^2$) and photon energy, ε, as our independent variables and to difference uniformly in the logarithm of these energies. The electron and photon number densities per unit energy are designated by $N_\gamma(\gamma)$ and $n_\varepsilon(\varepsilon)$. The two

kinetic equations can then be written

$$\frac{\partial N_\gamma}{\partial t}=\frac{\partial N_\gamma}{\partial t}\bigg|_{\rm PP}+\frac{\partial N_\gamma}{\partial t}\bigg|_{\rm C}+\frac{\partial N_\gamma}{\partial t}\bigg|_{\rm A}+Q(\gamma), \tag{1}$$

$$\frac{\partial n_\varepsilon}{\partial t}=\frac{\partial n_\varepsilon}{\partial t}\bigg|_{\rm PP}+\frac{\partial n_\varepsilon}{\partial t}\bigg|_{\rm C}+\frac{\partial n_\varepsilon}{\partial t}\bigg|_{\rm A}+\frac{\partial n_\varepsilon}{\partial t}\bigg|_{\rm E}+S(\varepsilon). \tag{2}$$

The subscripts PP, C, A, E stand respectively for pair production, Compton scattering, annihilation and escape. $Q(\gamma)$, $S(\varepsilon)$ are source functions describing impulsive acceleration of relativistic electrons and irradiation by soft photons. [Note that $Q(\gamma)$ is a source of electrons and positrons in equal number.]

2.2 PAIR PRODUCTION

This is assumed to be entirely due to photon–photon collisions. The interaction cross-section is approximated by a rectangular function of amplitude $0.2\,\sigma_{\rm T}$ extending from a threshold at $\varepsilon_1\varepsilon_2=2$, where ε_1 is the energy of the γ-ray ($\varepsilon_1>\sqrt{2}$) and ε_2 that of the X-ray ($\varepsilon_2<\sqrt{2}$), to $\varepsilon_1\varepsilon_2=10$. Then the rate of absorption of γ-rays is given by

$$\frac{\partial n_\varepsilon(\varepsilon_1)}{\partial t}\bigg|_{\rm PP}=-0.2n_\varepsilon(\varepsilon_1)\sigma_{\rm T}c\int_{2/\varepsilon_1}^{\min(10/\varepsilon_1,\varepsilon_1)} n_\varepsilon(\varepsilon_2)\,d\varepsilon_2; \qquad \varepsilon_1\geqslant\sqrt{2}. \tag{3}$$

The resulting electrons are assumed to share the energy of the absorbed photons equally so that (*cf.* Bonometto & Rees 1971)

$$\frac{\partial N_\gamma}{\partial t}\bigg|_{\rm PP}=0.4\,\sigma_{\rm T}c\int_{\sqrt{2}} d\varepsilon_1 n_\varepsilon(\varepsilon_1)\int_{2/\varepsilon_1}^{\min(10/\varepsilon_1,\varepsilon_1)} d\varepsilon_2 n_\varepsilon(\varepsilon_2)\,\delta\left(\gamma-\frac{\varepsilon_1+\varepsilon_2}{2}\right). \tag{4}$$

2.3 COMPTON SCATTERING

We deal with Compton scattering by considering two separate electron distributions. One is relativistic and inverse Compton scatters photons according to

$$\varepsilon_{\rm f}=\gamma^2\varepsilon_{\rm i} \tag{5}$$

where $\varepsilon_{\rm f}$ and $\varepsilon_{\rm i}$ are the final and initial photon energies, respectively. (The factor of 4/3, which would be present if the radiation field were isotropic, is omitted.) A Klein–Nishina cut-off is applied such that photons of energy, ε, are scattered by electrons of energy, γ, only if $\varepsilon\gamma<1$.

The photon distribution function evolves according to

$$\frac{\partial n_\varepsilon(\varepsilon_{\rm f})}{\partial t}=\sigma_{\rm T}c\int d\varepsilon_{\rm i} n_\varepsilon(\varepsilon_{\rm i})\int d\gamma N_\gamma(\gamma)\,\delta(\varepsilon_{\rm f}-\gamma^2\varepsilon_{\rm i}) \tag{6}$$

Electrons cooled by inverse Compton scattering to sub-relativistic energies, $\gamma\sim1$, are consigned to a thermal bin. We assume that Coulomb collisions (and other interactions) within this bin rapidly establish a Maxwellian velocity distribution. This will generally occur if the resulting temperature, T (measured in units of $m_{\rm e}c^2/k$) is low i.e. $T\lesssim0.1$. This occasions some inaccuracy in the treatment of sub-relativistic electrons before they are thermalized, but relatively little energy is involved, so the effect is small. Comptonization by the thermal

(sub-relativistic) electrons, of density N_0, is approximated by an energy shift per scattering

$$\frac{\Delta\varepsilon}{\varepsilon_i}=4T-\frac{\varepsilon_i}{1+\varepsilon_i}; \tag{7}$$

so

$$\varepsilon_f=\varepsilon_i+\Delta\varepsilon. \tag{8}$$

The first term in equation (7) describes Fermi acceleration of the photons by the moving electrons; the second term accounts for energy loss due to electron recoil. The electron temperature, T, is adjusted so that energy is conserved each time the thermal electron distribution is changed. The dispersion, can be neglected, in the scattering if the underlying spectrum is very broad. It does, however, exaggerate the sharpness of lines and of any Wien peak. This approach to Comptonization gives fair agreement with the results of Sunyaev & Titarchuk (1980).

2.4 ELECTRON DISTRIBUTION FUNCTION

As the inverse Compton cooling time for a relativistic electron is much shorter than the other time-scales in the problem, we can assume that the electron distribution function achieves a steady state in each time step. High-energy particle injection and pair production are balanced by the inverse Compton losses to give

$$N_\gamma=\frac{\int_\gamma^\infty d\gamma'[Q(\gamma')+(\partial N_\gamma/\partial t)(\gamma')|_{PP}]}{(\gamma^2-1)\int d\varepsilon\,\varepsilon n_\varepsilon(\varepsilon)\sigma_T c}. \tag{9}$$

In fact, the cooling times lengthen at mildly relativistic energy and equation (9) is not a very good approximation.

2.5 PAIR ANNIHILATION

As the relativistic electron cooling times are so short, much less than their annihilation time [$t_{cool}/t_{ann}\simeq N_0 m_e c^2/(\gamma^2 U_r)<1/(\gamma^2 l_x)$ where U_r is the photon energy density], we need only consider annihilation by the thermal electrons. This is assumed to occur at a rate

$$\left.\frac{\partial N_0}{\partial t}\right|_A=-2\left(\frac{N_0}{2}\right)^2\frac{3}{8}\sigma_T c. \tag{10}$$

The resultant photons are assumed to have equal energy $\varepsilon_a=1+3T/2$ according to

$$\left.\frac{\partial n_\varepsilon(\varepsilon)}{\partial t}\right|_A=\tfrac{3}{16}N_0^2\sigma_T c\,\delta(\varepsilon-1-\tfrac{3}{2}T). \tag{11}$$

The contribution to the annihilation by electrons which have not yet reached the thermal bin can be ignored.

Numerically, the δ-function is broadened by the finite resolution in energy. (Our grid spacing means that the apparent width approximates the thermal width in the runs which we present, i.e. $T\simeq 10^{-2}$.) In practice, the linewidth will be dictated by motions with speeds of c within the source

region and the bin will probably be smeared out. As the line carries relatively little power, it does not affect the shape of the continuum.

2.6 ESCAPE

Radiation transfer is handled by using a very simple escape probability formulism

$$\left.\frac{\partial n_\varepsilon}{\partial t}\right|_{\mathrm{E}} = -\frac{n_\varepsilon}{1+\tau_0}\frac{c}{R}, \tag{12}$$

where $\tau_0 = N_0 \sigma_{\mathrm{T}} R$ for $\varepsilon < 1$ is the scattering optical depth. Here R is defined to be the half-thickness of the slab or the radius of the cylinder or sphere. The mean rate of escape from even a stationary source will depend sensitively on its shape as well as on the distribution of scattering electrons* (see e.g. Payne 1980; Sunyaev & Titarchuk 1980). In practice, equation (12) can be used to define the 'average' source size, R, and photon density n_ε used in our model equations. The emergent spectrum is given by $-(\partial n_\varepsilon/\partial t)|_{\mathrm{E}}$. This simple formula (12) fails at energies $\varepsilon > 1$, due to the Klein–Nishina reduction in the scattering cross-section and when the photon–photon pair-production opacity exceeds the scattering opacity. This mainly affects the predicted γ-ray flux, especially at high luminosities, but has little influence on the conditions inside the source or the X-ray spectrum.

2.7 INJECTION

Photons must be injected into the source to replace those that escape. In this paper we are mainly concerned with models in which there is a strong source of UV photons (e.g. an accretion disc, $\varepsilon_1 \sim 10^{-4}$) or photons emitted as self-absorbed synchrotron or cyclotron radiation at lower energies ($\varepsilon_1 \sim 10^{-7}$). We assume a monoenergetic radiation source of energy $\varepsilon_1 \ll 1$. As discussed in the Introduction, electrons are assumed to be injected at high energies at $\gamma_{\max} \simeq 10^3$. These replenish the energy carried off by the escaping radiation.

The dimensionless radiation and electron-injection powers are given by

$$\dot{U}^{\mathrm{rad}} = \int \varepsilon S(\varepsilon)\, d\varepsilon; \tag{13}$$

$$\dot{U}^{\mathrm{el}} = \int \gamma Q(\gamma)\, d\gamma. \tag{14}$$

2.8 THE COMPACTNESS PARAMETER

We have already defined observational compactness parameters by

$$l_{\mathrm{x},\gamma} = \frac{F_{\mathrm{x},\gamma}\,\sigma_{\mathrm{T}} R}{m_{\mathrm{e}} c^3}, \tag{15}$$

where $F_{\mathrm{x},\gamma}$ is the inferred X-ray or γ-ray flux emerging from the surface of the source. A more appropriate compactness parameter for our computations, l, makes use of the power per unit volume injected in relativistic electrons, $\dot{U}^{\mathrm{el}}$,

$$l = \frac{\dot{U}^{\mathrm{el}} \sigma_{\mathrm{T}} R^2}{m_{\mathrm{e}} c^3}. \tag{16}$$

* In the diffusion approximation ($\tau_0 \gg 1$) we have $\partial n_\varepsilon/\partial t|_{\mathrm{E}} = -g_{\mathrm{T}} n_\varepsilon c/R\tau_0$, where $g_{\mathrm{T}} = \pi^2/12$, $j_{0,1}^2/3 \simeq 1.93$ and $\pi^2/3$ for a slab, a cylinder and a sphere, respectively, correcting these authors in the cylindrical case.

We now define $f_{x,\gamma}$ to be the fraction of the total source power escaping as X-rays (γ-rays). The flux at the surface of the source is then given by

$$F_{x,\gamma}=(\dot{U}^{el}+\dot{U}^{rad})(R/D)f_{x,\gamma}, \tag{17}$$

where $D=1, 2, 3$ for slab, cylinders and spheres respectively, and R is defined in Section 2.6. This procedure relates the theoretical and observational compactness parameters through equation (15).

3 Results

3.1 NUMERICAL PROCEDURE

We specify the electron and photon injection spectra and then solve for the time evolution of the photon distribution function $n_\varepsilon(\varepsilon)$, substituting equations (3), (6), (11) and (12) using equation (9) for the electron distribution function. At each time step the sub-relativistic electron density N_0 is increased by the electrons cascading down from higher energy and reduced by pair annihilation [equation (10)]. The time step must be smaller than the shorter of the light crossing time and the Thomson time for numerical stability and typical time steps are in the range $(0.01–0.05)R/c$. We compute the emergent spectrum from equation (12).

3.2 SPECTRUM

The case $\dot{U}^{rad}\gg U^{el}$, $\tau_0<1$ has been investigated analytically by Zdziarski & Lightman (1985). They found that the X-ray spectrum, for $\varepsilon<1$, was approximately a power law with $0.5\lesssim\alpha\lesssim1.0$. We find that in the more general case this result still holds over that spectral band where the effect of Compton scattering by the thermal electron component is not apparent; the size of this band depends on ε_1, $\dot{U}^{rad}/\dot{U}^{el}$ and τ_0. At low energies, scattering by the thermal electrons creates a power-law tail to the soft input photons. For $\dot{U}^{rad}>\dot{U}^{el}$ the spectral index of this tail $\alpha_s\gtrsim1+\dot{U}^{rad}/\dot{U}^{el}$. It dominates the spectrum up to an energy ε_c where it intersects the main power-law spectrum produced by the relativistic electrons. At higher energies Compton recoil on the cold electrons causes the spectrum to break at an energy $\varepsilon\simeq1/\tau_0^2$ if $\tau_0<1$ (the thermal electrons cool until y, defined as $4T\tau_0^2$, $\lesssim1$)*. The numerical results somewhat over-emphasize this break due to the assumption of a Thomson scattering cross-section up to $\varepsilon=1$.

Some results of computations are listed in Table 1. A wide (hundred fold) range of input parameters in the form of l and $\dot{U}^{rad}/\dot{U}^{el}$ was investigated; the resulting range in Thomson depth is shown in Table 1. For $\gamma_{max}=10^3$, and $\varepsilon_1=10^{-4}$ the 2–10 keV spectral index α (Table 1) is remarkably constant between ~0.7 and 0.8 until the Compton temperature has dropped considerably below 2 keV. α increases slightly with increasing γ_{max}. The observation that $\alpha\simeq0.7$ in active galaxies is explained by our results if $10^2\lesssim\gamma_{max}\lesssim10^4$; the source of soft photons may be the 'UV bump', $1\,eV\lesssim\varepsilon_1\lesssim100\,eV$.

Overall spectra for $l=10$ and $\dot{U}^{rad}/\dot{U}^{el}=0.1$ and 10 are shown in Fig. 1. It can be seen that the 0.5–50 keV spectral slope is little affected by $\dot{U}^{rad}/\dot{U}^{el}$ while τ_0 ranged from 1.54 to 2.30. Fixing $\dot{U}^{rad}/\dot{U}^{el}$ at 1, we show spectra for $l=1$, 10, 100 and 1000 in Fig. 2, as τ_0 ranged from 0.22 to 19.3. Note that $\tau_0\propto l^{1/2}$ (Guilbert *et al.* 1983). (The spectral shape is little changed if σ_T is taken to be zero above $\varepsilon=1$, as a crude approximation of the Klein–Nishina cut-off.) We have also carried

*Note that the thermal electron temperature is always much less than 1. The maximum possible value is the Compton temperature for a power-law spectrum of index 0.5 which is 0.14 (74 keV) and so in general we expect $(1+\dot{U}^{el}/\dot{U}^{rad})\varepsilon_1<T<0.14$ (Guilbert 1986).

Table 1.

ℓ	U^{rad}/U^{el}	ϵ_1	γ_{max}	τ_0	T	y+	x	α	No.
10	0.1	10^{-4}	10^3	2.30	2.7×10^{-2}	0.57	0.099	0.78	1
10	1	"	"	1.75	1.1×10^{-2}	0.13	0.057	0.76	2
10	10	"	"	1.54	1.9×10^{-3}	0.018	0.044	0.77	3
1	1	"	"	0.22	8.0×10^{-2}	0.013	0.008	0.66	4
100	1	"	"	5.97	2.1×10^{-3}	0.30	0.067	0.97	5
1000	1	"	"	19.26	5.1×10^{-4}	0.76	0.069	1.71	6
10	1	10^{-4}	10^2	1.34	1.7×10^{-2}	0.12	0.033	0.62	7
10	1	10^{-5}	10^4	1.64	1.1×10^{-2}	0.12	0.050	0.78	8
10	1	10^{-7}	10^6	1.64	9.1×10^{-3}	0.097	0.050	0.97	9
10	1	9×10^{-5}	10^4	1.95	1.1×10^{-2}	0.017	0.071	0.87	10
10	1	10^{-7}	10^3	0.52	7.6×10^{-3}	0.008	0.005	0.51	11
1.17	10	2.7×10^{-5}	4.0×10^3	0.271	8.5×10^{-3}	2.5×10^{-3}	-	0.67	12
4.77	10	"	2.7×10^4	0.970	3.5×10^{-3}	1.3×10^{-2}	-	0.91	13
100	1	10^{-7}	10^2	-	-	-	-	-	14
4.77	10	2.7×10^{-5}	2.7×10^4	0.98*#	8.9×10^{-3}	8.9×10^{-3}	-	0.88#	15
4.77	10	2.7×10^{-5}	2.7×10^4	1.93*	-	-	-	0.96	16

Notes:

+ y is the Compton y-parameter ($=4T\tau_0^2$).

* No thermal Comptonisation.

\# Photons escape on crossing time.

out calculations assuming lower values of ε_1 such as 10^{-7} (Fig. 3; runs 9, 11). This is also a crude representation of the effect of soft photons produced by self-absorbed synchrotron radiation.

A comparison has been made with the results of Zdziarski & Lightman (1985), who ignore the effects of the thermal electrons. Runs 12 and 13 (Table 1) are at the appropriate values of l and provide a direct comparison. When $\tau_0<0.3$ (e.g. run 12), our results are similar. However, when $\tau_0>0.3$ (e.g. run 13) we obtained a steeper X-ray spectrum. To investigate this difference we removed the effects of thermal Comptonization (run 16) which has increased both α and τ_0. This was due to an increased pair efficiency associated with a lack of down-scattering over $1/\tau_0^2<\varepsilon<1$. We next eliminated all scattering by thermal electrons by setting $(\partial n_\varepsilon/\partial t)_E=-n_\varepsilon$ (run 15), thereby reducing the soft photon density and hence pair opacity τ_{pp}. Good agreement is now obtained with the results by Zdziarski & Lightman (1985); the remaining discrepancies are due to our different algorithms for estimating τ_{pp}, the photon–photon optical depth. This comparison shows that the effects of electron scattering by thermal electrons are significant when $\tau_0>0.3$.

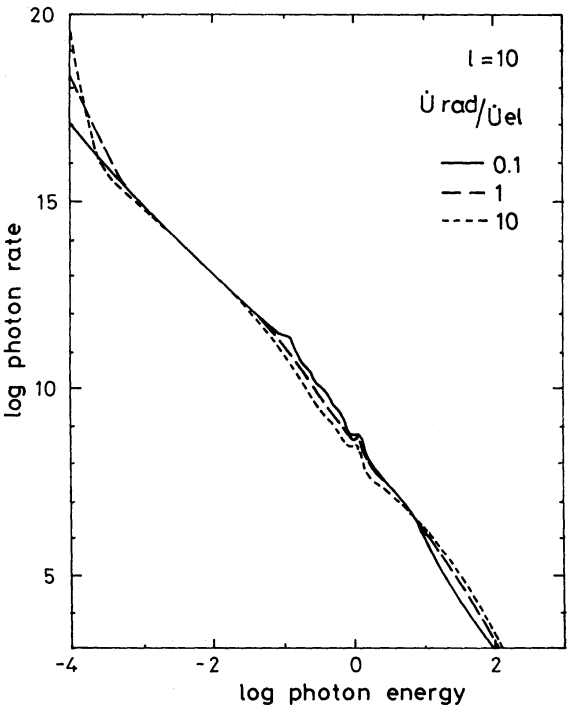

Figure 1. Emergent photon number spectra for runs 1–3. $2.3 \leqslant \tau_0 \leqslant 1.54$. Photon energy is in units of $m_e c^2$. X-ray photon index, $(\alpha+1)$, lies between 1.76 to 1.78. Note the weak annihilation feature at $\varepsilon \approx 1$ and the beginnings of a Wien peak at $\varepsilon \approx 0.1$ in the hardest spectrum. The slight oscillations in the spectrum between these two features are a result of the lack of dispersion in our treatment of Compton scattering and of the numerical grid.

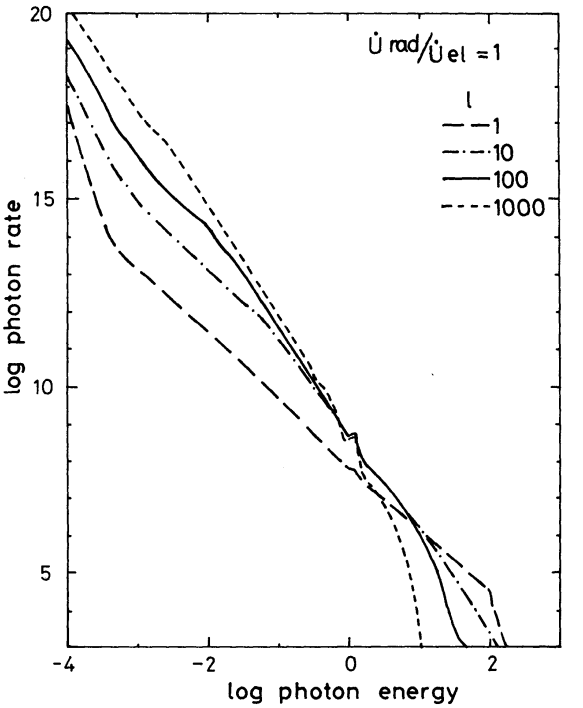

Figure 2. Emergent photon number spectra for runs 2, 4–6. $0.22 \leqslant \tau_0 \leqslant 19.26$. Compton scattering of hard X-rays by the cooled pair gas leads to a steepening of the X-ray spectrum above $\varepsilon \sim \tau_0 - 2$. Note that the most pair-dominated source exhibits the weakest γ-ray spectrum.

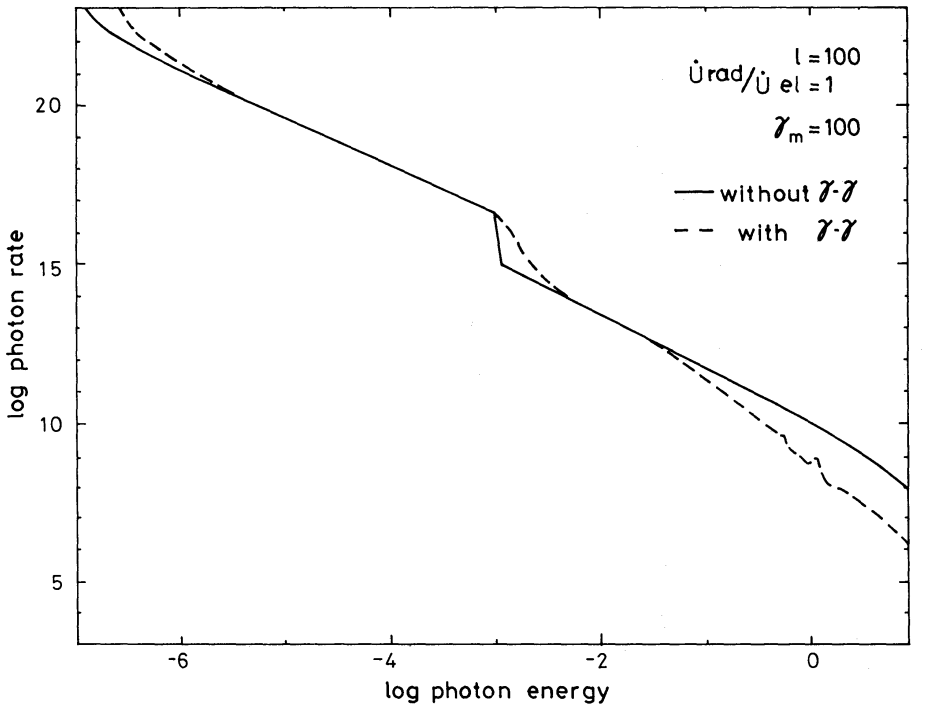

Figure 3. Emergent photon number spectrum for run 14 in which all pair effects are omitted. The first- and second-order inverse Compton spectra are evident, $\alpha=0.5$. The dashed line shows the change in spectrum when pair effects are included.

3.3 ANNIHILATION LINE

The annihilation line compactness parameter [*cf.* equation (15)] is

$$l_a \simeq \varepsilon_a n_a \sigma_T R, \tag{18}$$

where n_a is the photon density at the dimensionless line energy, $\varepsilon_a=1+3T/2$. In equilibrium, line photon creation is balanced by escape and scattering to lower energies by Compton recoil

$$\tfrac{3}{16} N_0^2 \sigma_T c \simeq n_a \left(\frac{N_0 \sigma_T c}{2} + \frac{c}{R} \right), \tag{19}$$

where we estimate the scattering cross-section as $\sigma_T/2$ at the line energy. (The exact scattering rate depends on T, see Guilbert 1986). Solving (19) we find

$$n_a \simeq \frac{3}{8} \frac{N_0 \tau_0}{\tau_0+2} \tag{20}$$

and

$$l_a \simeq \frac{3}{8} \frac{\varepsilon_a \tau_0^2}{\tau_0+2}. \tag{21}$$

So for $\tau_0<1$, $l_a \propto \tau_0^2 \propto l$, that is the line luminosity is just proportional to the hard input luminosity. For $\tau_0>1$, on the other hand, l_a is $3\varepsilon_a\tau_0/8$. The apparent saturation of the line luminosity, seen in Fig. 2 when $l>1$ is due to our escape approximation (12).

3.4 COMPTONIZATION

The numerical results indicate the presence of a small Wien bump at $\varepsilon \simeq 4T$. This is a result of not including energy dispersion in the Compton scattering. No Wien bump should be seen for $y<1$. The maximum value of $y \simeq \log(1+\dot{U}^{\rm el}/\dot{U}^{\rm rad})$ so, for $\dot{U}^{\rm rad} > \dot{U}^{\rm el}$, y can never be greater than unity. When $\dot{U}^{\rm rad} > \dot{U}^{\rm el}$, the thermal component will therefore have no significant effect on the spectrum in the energy range $\varepsilon_{\rm c} < \varepsilon < 1/\tau_0^2$.

3.5 PAIR PRODUCTION

A further parameter given in Table 1 is x, the mean number of pairs produced per $2m_{\rm e}c^2$ of energy of primary electrons above the threshold (Guilbert *et al.* 1983). For runs 1–10,

$$x = \tfrac{3}{16}\tau_0^2/l, \tag{22}$$

and ranges from 0.037 to 0.148, much less than the limit of 0.25 given by Svensson (1986). It is smallest for low l and high $\dot{U}^{\rm rad}/\dot{U}^{\rm el}$. $x \simeq 1$ would imply a complete pair cascade, which is unreasonable in the situations computed here where much of the energy in pairs goes into inverse Compton scattering. As expected, increasing the relative soft photon intensity in the source (high $\dot{U}^{\rm rad}/\dot{U}^{\rm el}$) leads to fewer hard scattered photons and thus fewer pairs. The mean energy of the primary spectrum (including the input photons) is the important factor.

3.6 VARIABILITY

There are three basic time-scales involved: the light crossing time, $t_{\rm c} = R/c$; the Thomson time, $t_{\rm T} = R/(\tau_0 c)$; and the escape time from the source, $t_{\rm e} = (1+\tau_0)R/c$. The time-scales associated with the relativistic electrons are much shorter than these, if $l_{\rm x} > 1$. We note that the scattering optical depth τ_0 which should be used to compute the escape time is generally the value it has *after* a change has taken place. For example if high energy injection were suppressed in a source with $\tau_0 > 1$ the escape time would be $\sim R/c$ and not $(1+\tau_0)R/c$ since the pairs annihilate on a Thomson time.

If $\tau_0 < 1$ then we can see that all the time-scales are R/c except the Thomson time, so the thermal plasma has no effect on the variability. The time-scale for pair production and annihilation is the Thomson time, however, and in this case the annihilation line varies on a longer time-scale than the rest of the spectrum.*

When $\tau_0 < 1$ then $t_{\rm e} < t_{\rm c}$ and the pairs have a significant effect on the spectral variability. Figs 4 and 5 show the effect of switching the source on and off (both $\dot{U}^{\rm rad}$ and $\dot{U}^{\rm el}$) and of varying its luminosity by 50 per cent. The soft photons $\varepsilon < 1/\tau_0^2$ have an asymmetrical behaviour requiring $(1+\tau_0)$ crossing times to reach maximum flux but only one crossing time to switch off. The hard photons $\varepsilon > \varepsilon_{\rm a}$ are unaffected by the pairs and so their time-scale is $t_{\rm c}$. The hard ($\varepsilon \gg 1$) part of the spectrum is the only part which always varies on a time-scale directly related to the source size, $t_{\rm c}$.

The pairs establish themselves on a Thomson time $t_{\rm T}$, when $t_{\rm T} < t_{\rm c}$, changes in the annihilation line luminosity are small. If the source switches off then at times $t > t_{\rm c}$, the pair luminosity is proportional to $1/t^2$. Consequently, the line luminosity then dominates and this might provide the best opportunity for detecting the presence of pairs in highly compact luminous sources. For photon energies $1/\tau_0^2 < \varepsilon < \varepsilon_{\rm a}$ Compton scattering determines the distribution, and equilibrium cannot be established on time-scales shorter than $t_{\rm c}/\tau_0\varepsilon$.

In Fig. 5, the flux of ~2 keV X-rays *anti-correlates* with the input luminosity since an increase in power rapidly produces more cooled pairs which trap the X-rays and so decrease their emergent

* Since the final spectrum depends on the equilibrium relativistic pair cascade distribution which establishes itself on a Thomson time, small changes will be seen throughout the spectrum on that time-scale.

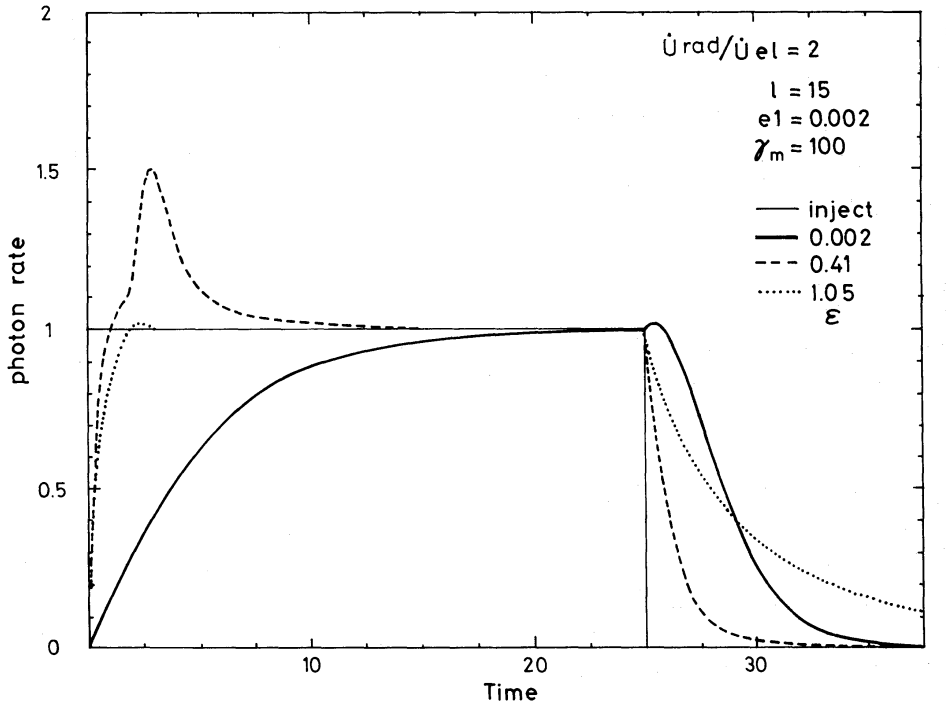

Figure 4. Emergent photon flux for $\varepsilon=0.002, 0.41$ and 1.05 (the annihilation feature) when the injected electrons and photons are abruptly switched on at time=0 and off after 25 light crossing times. The fluxes have been normalized to their value just before switch-off. Note that the annihilation feature decays more slowly than the other spectral points.

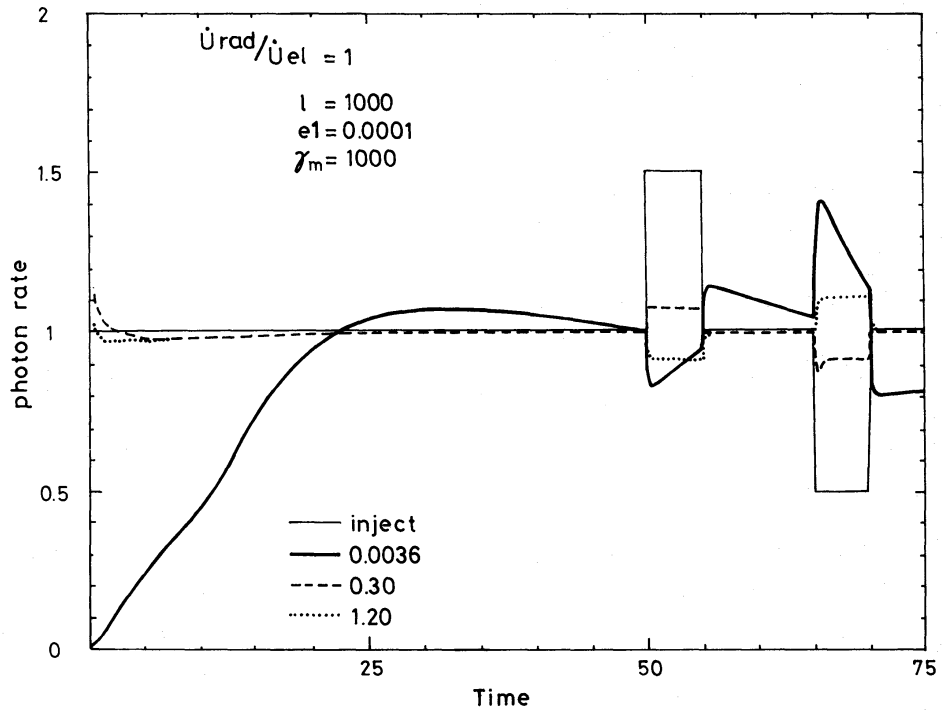

Figure 5. Emergent photon number flux for $\varepsilon=0.0036$ (~2 keV), 0.3 and 1.2 (the annihilation feature) for the parameters of run 6. The injection source is abruptly switched on at time=0, increased temporarily by 50 per cent at time=50 and decreased at 75. The spectra are normalized to their values just before the increase. The hard X- and γ-rays increase to a value ~4 on this scale (not shown) immediately after switch-on before photon–photon collisions and Compton scattering remove them. Note that the 2 keV X-rays are anti-correlated with the injected power.

flux. Conversely a reduction in input power leads to a rapid reduction in the pair density (at rate given in equation 10), and an emergent burst of (previously trapped) X-rays. The Thomson opacity of the pairs causes the photons to be stored. The observed source luminosity after a rapid decrease in injected power can temporarily be a factor of up to $\frac{3}{16}\tau_0$ greater than the previous injected power. Pair-dominated sources may thus show the most dramatic variations, which may exceed the efficiency limit (Fabian 1979). Since $\tau \propto \sqrt{\dot{U}^{el}}$ (Guilbert *et al.* 1983), a change in $\dot{U}^{el}$ by a factor, f, leads to a change in F_{obs} by a factor $f^{-0.5}$, in good agreement with Fig. 5. An abrupt switch off of the injected power in the calculation shown in Fig. 5 led temporarily to a fourfold increase in the 2 keV flux.

3.7 COMPARISON WITH OBSERVATIONS

Some comparison with observational work is appropriate. Unfortunately, there is little information on the hard X-ray spectra of active galaxies. The confusion concerning the spectrum of the Seyfert 1 galaxy NGC 4151 (Perotti *et al.* 1981) may be explainable as variability in a source such as that modelled here. The decreasing γ-ray flux, observed by Baity *et al.* (1984) as the 2–100 keV X-ray flux increased without a change of spectral shape, is similar to that shown in Fig. 2. The overall spectra for $l=10$ are similar to those of Cygnus X-1 (Sunyaev & Trümper 1979; Nolan *et al.* 1981) and the distinctive spectral state change is approximately reproduced by increasing $\dot{U}^{rad}/\dot{U}^{el}$ through unity at fixed l (Fig. 6). This spectral softening at the expense of the hard flux could arise if much of the injected energy is radiated as soft photons, perhaps as synchrotron radiation.

Rapid variability in non-thermal pair sources allows hard primary radiation to emerge briefly. The non-thermal underlying nature of the primary power source is soon cloaked from view by the 'thermal' pairs. This may be important in the interpretation of hard radiation from γ-ray bursts

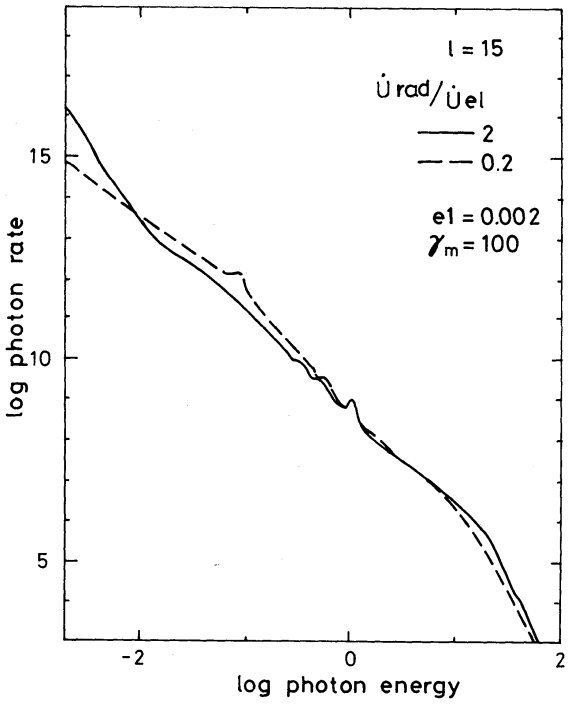

Figure 6. Emergent photon number spectra for the same injected electron power, U^{el}, but the proportion of injected photons varied by a factor of 10. The X-ray spectrum steepens when the injected photon power is large. The spectra resemble the two states of Cyg X-1.

(see e.g. Matz *et al.* 1985). The steady-state spectra shown in Fig. 2 are similar in shape over the 20–500 keV range to γ-ray bursts.

The ceiling of the observable steady-state continuum flux at $\varepsilon \sim 1$ is a characteristic of pair sources. We stress that the source *appears* softer and with fewer hard photons as pairs become more important (Fig. 2). Observationally this means that pairs may dominate the radiation transport in those X-ray sources where they are least expected. Source variability can become more pronounced as pairs are rapidly created or annihilated, trapping or releasing the X-rays.

If active galactic nuclei contribute significantly to the X-ray background at photon energies of a few keV, then their compactness parameters must be large enough that their spectra break at high energies (*cf.* Section 3.2) before exceeding the γ-ray background.

4 Conclusions

We have made a simple model of an X-ray/γ-ray source involving non-thermal electrons with Lorentz factor $\gamma_{\max}=10^3$ and photons with energy $\varepsilon_1 \simeq 50$ eV (which may be thermal or non-thermal). Under a wide range of conditions, an electron–positron plasma with scattering optical depth $\tau_0 > 1$ is produced. The steady X-ray flux emerging from this source has a 2–10 keV spectral index $\alpha \simeq 0.7$ similar to that measured in many active galactic nuclei. The emergent γ-ray flux can be misleadingly low, especially in the most pair-thick sources. Large amplitude X-ray variability, which may temporarily be in the opposite sense to that of the injected power, may occur in these sources.

The model equations that we have solved embody extremely simple approximations to the various relevant cross-sections. Our results are most sensitive to our prescription for handling radiative transfer and Comptonization. We plan to develop a more detailed model which we believe will verify that the main observable features of our model are insensitive to the particular approximations that we have made.

Acknowledgments

We thank R. Svensson for discussions. RB acknowledges financial support under National Science Foundation grants AST82-13001 and AST84-75355. LC acknowledges support under the Caltech Summer Undergraduate Research Fellowship Program. ACF thanks the Royal Society for support. The research of ESP is supported in part by a Presidential Young Investigators Award, NSF AST84-51725 and a grant from the Exxon Education Foundation.

References

Baity, W. A., Mushotzky, R. F., Worrall, D. M., Rothschild, R. E., Tennant, A. F. & Primini, F. A., 1984. *Astrophys. J.*, **279,** 555.

Barr, P. & Mushotzky, R. F., 1986. Preprint.

Blandford, R. D., 1984. *Ann. N.Y. Acad. Sci.*, **422,** 303.

Blandford, R. D. & McKee, C. F., 1977. *Mon. Not. R. astr. Soc.*, **180,** 343.

Blandford, R. D. & Znajek, R. L., 1977. *Mon. Not. R. astr. Soc.*, **179,** 433.

Bonometto, S. & Rees, M. J., 1971. *Mon. Not. R. astr. Soc.*, **152,** 21.

Cavallo, G. & Rees, M. J., 1978. *Mon. Not. R. astr. Soc.*, **183,** 359.

Elvis, M. & Lawrence, A., 1985. *Astrophysics of Active Galaxies and Quasi-Stellar Objects,* p. 289, ed. Miller, J. S., University Science Books, Mill Valley, California.

Fabian, A. C., 1979. *Proc. R. Soc.*, **366,** 449.

Fabian, A. C., 1984. *X-ray and UV Emission from Active Galactic Nuclei,* p. 232, eds Brinkmann, W. L. & Trümper, J., MPE report 184, MPIFE, Garching.

Fabian, A. C., 1985. *Active Galactic Nuclei,* p. 221, ed. Dyson, J., Manchester University Press.

Guilbert, P. W., 1986. *Mon. Not. R. astr. Soc.,* **218,** 171.
Guilbert, P. W., Fabian, A. C. & Rees, M. J., 1983. *Mon. Not. R. astr. Soc.,* **205,** 593.
Herterich, K., 1974. *Nature,* **250,** 311.
Jelley, J. V., 1966. *Nature,* **211,** 472.
Kazanas, D., 1984. *Astrophys. J.,* **287,** 112.
Lawrence, A. , Watson, M. G., Pounds, K. A. & Elvis, M., 1985. *Mon. Not. R. astr. Soc.,* **217,** 685.
Matz, S. M., Forrest, D. J., Vestrand, W. T., Chupp, E. L., Share, G. H. & Rieger, E., 1985. *Astrophys. J.,* **288,** L37.
Mushotzky, R. F., 1982. *Astrophys. J.,* **256,** 92.
Nolan, P. L., Gruber, D. E., Knight, F. K., Matteson, J. L., Rothschild, R. E., Marshall, F. E., Levine, A. M. & Primini, F. A., 1981. *Nature,* **293,** 275.
Payne, D. G., 1980. *Astrophys. J.,* **237,** 951.
Perotti, F., Della Ventura, A., Villa, G., Di Cocco, G., Bassani, L., Butler, R. C., Carter, J. N. & Dean, A. J., 1981. *Astrophys. J.,* **247,** L63.
Petre, R., Mushotzky, R. F., Krolik, J. H. & Holt, S. S., 1984. *Astrophys. J.,* **280,** 499.
Phinney, E. S., 1983. *PhD thesis,* Cambridge University.
Rothschild, R. E., Mushotzky, R. F., Baity, W. A., Gruber, D. E., Matteson, J. L. & Peterson, L. E., 1983. *Astrophys. J.,* **269,** 423.
Sunyaev, R. A. & Titarchuk, L. G., 1980. *Astr. Astrophys.,* **86,** 121.
Sunyaev, R. A. & Trümper, J., 1979. *Nature,* **279,** 509.
Svensson, R., 1986. *Hydrodynamics in Stars and Compact Objects, IAU Coll. No. 89,* in press.
Tennant, A. F., Mushotzky, R. F., Boldt, E. A. & Swank, J. H., 1981. *Astrophys. J.,* **251,** 15.
White, N. E., Fabian, A. C. & Mushotzky, R. F., 1984. *Astr. Astrophys.,* **133,** L9.
Zdziarski, A. A & Lightman, A. P., 1985. *Astrophys. J.,* **294,** L79